ACS APPLIED MATERIALS & INTERFACES

Research Article

www.acsami.org

Enhanced Charge Transfer Kinetics of CdSe Quantum Dot-Sensitized Solar Cell by Inorganic Ligand Exchange Treatments

Hyeong Jin Yun,[†] Taejong Paik,[†] Michael E. Edley,[§] Jason B. Baxter,[§] and Christopher B. Murray*[,†,‡]

[†]Department of Chemistry and [‡]Department of Materials Science and Engineering University of Pennsylvania, Philadelphia, Pennsylvania 19104, United States

[§]Department of Chemical and Biological Engineering, Drexel University, Philadelphia, Pennsylvania 19104, United States

Supporting Information

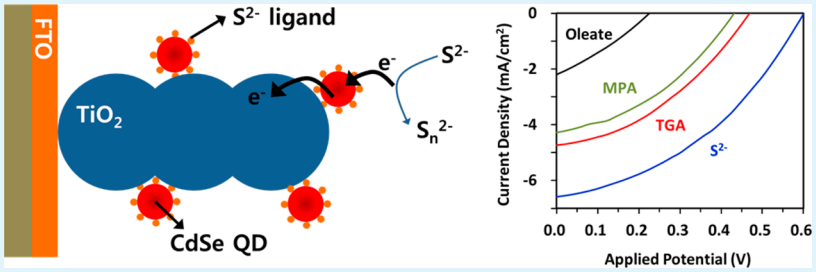

ABSTRACT: Enhancement of the charge transfer rate in CdSe quantum dot (QD) sensitized solar cells is one of the most important criteria determining cell efficiency. We report a novel strategy for enhancing charge transfer by exchanging the native, long organic chain to an atomic ligand, S^{2-}, with a simple solid exchange process. S^{2-}-ligand exchange is easily executed by dipping the CdSe QDs sensitized photoanode into a formamide solution of K_2S. The results show that this exchange process leads to an enhancement of the electronic coupling between CdSe QD and TiO_2 by removing the insulating organic barrier to charge transfer, while maintaining its quantum confined band structure. This treatment significantly increases the charge transfer rate at the interfacial region between CdSe QDs and TiO_2 as well as between the CdSe QDs and Red/Ox coupling electrolyte, as verified by time-resolved photoluminescence and electrochemical impedance spectroscopy measurements. Finally, the S^{2-}-treated photoanode exhibits a much higher photovoltaic performance than the conventional MPA or TGA-capped CdSe QDs sensitized solar cell. The findings reported herein propose an innovative route toward harvesting energy from solar light by enhancing the carrier charge transfer rate.

KEYWORDS: *CdSe QDs, quantum dot sensitized solar cell, ligand exchange, charge transfer rate*

INTRODUCTION

Quantum dot-sensitized solar cells (QDSSC) have attracted considerable interest as next-generation solar cells with using various semiconductor quantum dots (QDs) such as CdSe,[1−4] CdS,[1,2,5] CdTe,[1,2] and so on.[1,2,6] A QDSSC is a typical liquid junction-based photovoltaic cell which is similar to the dye sensitized solar cell, except that QDs are used as sensitizers instead of organic dyes to generate photo-excited carriers. Light absorption in solar cells is easily managed by controlling the size and shape of QDs, as the band gap of QDs is tunable because of the quantum-confinement effect.[7−11] Moreover, the high extinction coefficient of QDs (e.g., ε of 4 nm CdSe is 2.15 $\times 10^5$ cm^{-1} M^{-1}) results in the production of a large quantity of excited carriers in QDSSC.[12] These unique features of QDs enable them to be used as light sensitizers to harvest energy effectively in a liquid junction based-solar cell.

Electron transfer occurs at the interfaces between both solid−solid and solid−liquid junctions in the device. Hence, the charge transfer dynamics at these interfaces, for example, QDs and wide band semiconductors (TiO_2, ZnO, and so on) and QDs and the Red/Ox coupling electrolyte, are critical factors determining device performance and overall solar cell efficiency. Various methods to fabricate a QD-based photoanode have been introduced in order to increase coupling at the interfacial region, such as successive ionic layer adsorption and reaction (SILAR),[4,13−17] chemical bath deposition (CBD),[5,18,19] electrophoretic deposition (EPD),[20−23] linker-assisted assembly,[24,25] and electrodeposition.[26] Among the various techniques, in situ formation of QDs on a wide band semiconductor, such as SILAR and CBD methods has been predominantly used for the fabrication of the photoanode. Typically, in both methods, quantum dot sensitizers are grown in situ on the oxide layer by immersing the oxide coated electrodes into the solution containing precursor ions. This direct growth of sensitizers on the photoanode provides strong electronic coupling between the oxide layer and QDs. On the other hand, the deposition of pre-synthesized QDs, for example, EPD and linker assisted assembly, allows their size and shape to be more

Received: January 7, 2014
Accepted: January 21, 2014
Published: January 21, 2014

   dx.doi.org/10.1021/am500026a | ACS Appl. Mater. Interfaces 2014, 6, 3721−3728

precisely controlled than in situ growth. However, the presence of long organic ligands on the QD surface, which are used to control growth as well as to stabilize QDs as a colloidal solution, significantly inhibits the charge transfer at the interfacial region leading to inefficient solar cells (Scheme 1a).

Scheme 1. Schematic Diagram of Charge Transferring at the Interfacial Region in QDSSC Based on Colloidal CdSe QDs Capped by (a) Long Organic Chain, Oleate; and (b) Atomic Level Inorganic Ligand, S^{2-}

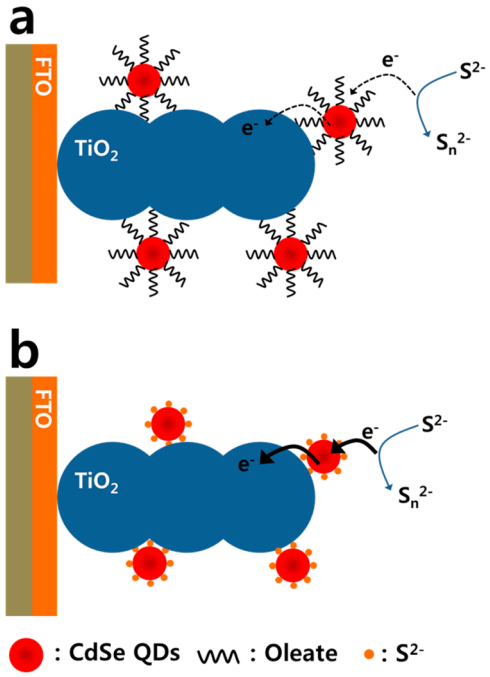

To increase the charge transfer rate at the interfacial region, we have studied a variety of ligand structures, such as inorganic ligands,[27−32] thioglycolic acid (TGA, $HSCH_2COOH$),[33] mercaptopropionic acid (MPA, $HSCH_2CH_2COOH$),[34,35] and other small organic ligands,[36−38] to decrease the distance between TiO_2 and quantum dots, and hence to increase the electronic coupling. Talapin et al. reported that nanocrystal can be stabilized by all-inorganic ligands including chalcogenides and hydrogen chalcogenide inorganic ions.[27−29] In particular, they show that the use of small inorganic ligands facilitates the charge transport between individual nanocrystals. Sargent et al. established an atomic ligand strategy by using halide anions to enhance electronic transport in a colloidal PbS quantum dot-based heterojunction solar cell.[30] Recently, these ligand exchange techniques have been applied to the QDs sensitized liquid junction solar cell by using TGA,[33] MPA,[34,35] and so on,[36−38] to exchange the long alkyl chain surfactant for a short ligand. Although these short organic ligands (MPA and TGA) help the photo-generated electrons to be transferred from the QDs to a wide band gap semiconductor, a barrier for photo-excited charge transfer at the interfacial region is not removed completely. Therefore, it is crucial to understand the effect of surface ligands on the charge transfer dynamics and overall solar cell performance.

Here, we investigate how changing the ligand on the surface affects the strength of coupling and resulting charge transfer dynamics between the CdSe QDs and TiO_2. The photoanodes for the QDSSC are fabricated by facile ligand exchange using a group of ligands with varying chain lengths; MPA, TGA, and S^{2-}. Short organic ligand exchange is accomplished by dipping a CdSe QDs-deposited photoanode into MPA or TGA, respectively. Inorganic ligand exchange using S^{2-} is achieved by submerging the photoanode into a formamide solution of K_2S, in a modification of the method reported by Talapin et al.[27] We observe that the type of the ligands on the QDs surface significantly influences photovoltaic performance, with shorter ligands enhancing the interfacial charge transfer rates. The injection rate of photo-excited electrons is much higher from S^{2-}-capped CdSe QDs into TiO_2 than from MPA or TGA-capped CdSe QDs under the irradiation of visible light (Scheme 1b), which is corroborated by time resolved photoluminescence (TRPL) and electrochemical impedance spectroscopy (EIS). It reveals that reducing the distance between the QDs and photoanode enhances the electron transfer rate, leading to an increase in overall photovoltaic cell efficiency.

EXPERIMENTAL DETAILS

Materials. The following chemicals were purchased and used as received. Cadmium oxide (CdO, 99.99 %), and potassium sulfide (K_2S, 95 %) were obtained from Strem Chemicals. 1-Octadecene (90 %), thioglycolic acid (98 %), 3-mercaptopropionic acid (99 %), and α-terpineol (97 %) were purchased from Acros Organics. Selenium powder (Se, 99.99 %), oleic acid (OLAC, 90 %), oleylamine (OLAM, 70 %), and acetic acid (99.7 %) were purchased from Sigma-Aldrich. Toluene (99.9 %), 2-propanol (99.9 %), ethanol (90 %), acetonitrile (99.9 %), and formamide (FA, 99.6 %) were obtained from Fisher Scientific. P25 TiO_2 and ethyl cellulose (5 % in toluene and ethanol) were purchased from Evonik Degussa Corporation and TCI, respectively. OLAC, OLAM, and FA were dried by standard procedures.

Synthesis of CdSe Quantum Dots. The CdSe QDs is prepared by modifying the synthesis method reported by P. Mulvaney et al.[39] In a typical reaction, 30 mL of octadecene (90%) is loaded into a 3-neck flask with 77 mg of CdO and 757 μL of OLAC. The mixture is heated to 250 °C under nitrogen until the solution gets clear, and then cooled down to 100 °C. Twenty-four milligrams of Se powder is added to the clear solution and the flask is held under vacuum for 1 h. After degassing the flask, it is heated to 240 °C under nitrogen. Once the reaction flask has reached 240 °C for 3 min, a degassed mixture of 1 mL of OLAM, 1 mL of OLAC, and 4 mL of ODE is injected to the reaction flask at the rate of 1 mL/min. Once the injection is completed, the reaction is allowed to continue at 240 °C for 30 min. The as-synthesized CdSe QDs are purified by precipitation with the addition of 2-propanol, and the precipitated QDs are redispersed in toluene to form stable colloidal dispersions.

Preparation of TiO_2 Paste. TiO_2 paste is prepared as reported previously.[40] Six grams of TiO_2 powder and 1 mL of acetic acid is mixed and ground in a mortar for 5 min. One milliliter of deionized water is added, whereas the TiO_2 in being ground in a mortar for 1 min, and this is repeated 5 times. Then, 1 mL of ethanol is added to the mixture while the slurry is ground in a mortar for 1 min, which is repeated 15 times. Then, 2.5 mL of ethanol is added to the mixture while being ground in a mortar for 1 min, which is repeated 6 times. This TiO_2 slurry is transferred to a beaker using 100 mL of ethanol. Twenty grams of α-terpineol is added to the TiO_2 slurry, after stirring and sonicating with an ultrasonic horn. Then, 6 g of

ethyl cellulose is added to the paste, after stirring and sonicating with an ultrasonic horn. Finally, TiO_2 paste is obtained after evaporating ethanol with a rotary evaporator.

Preparation of Photoanodes. Mesoporous TiO_2 films are prepared by layering TiO_2 paste using the doctor-blade technique on 2 mm thick fluorine-doped tin oxide (FTO) glass substrates (TCO22-7, Solaronix) with 7 Ω/cm^2 of sheet resistance. Before layering TiO_2 paste, the FTO glasses are cleaned sequentially with a detergent solution, DI water, and ethanol using an ultrasonic bath for 15 min during each step. Clean FTO glasses are obtained after treating in a UV-ozone system. After TiO_2 paste is layered on FTO glass, yielding an area of 0.25 cm^2, the electrodes are gradually sintered at a temperature of 325 °C for 5 min, 375 °C for 5 min, 450 °C for 15 min, and 500 °C for 15 min.

The electrophoretic bath is prepared by mixing 40 ml of CdSe QDs toluene solution (1×10^{-5} M) and 50 ml of acetonitrile. TiO_2/FTO and clean FTO electrodes, which are connected to positive and negative terminal of the power supply, respectively, are immersed in the prepared QD solution bath while keeping a distance of 1 cm. 100 V of DC voltage (EV215, Consort) is applied for 10 min, and then over-deposited CdSe QDs are rinsed with toluene. We repeated this cycle 6 times.

Ligand exchange is performed by dipping CdSe/TiO_2/FTO electrodes into each bath (MPA, TGA, K_2S solution in FA (10 mg/mL)) for 1 h. After exchanging, electrodes are cleaned with methanol.

Characterization of Photoanode. Transmission electron microscopy (TEM) images are recorded using a JEOL-1400 TEM equipped with a SC1000 ORIUS CCD camera operating at 120 kV. Scanning electron microscopy (SEM) is performed on a JEOL 7500F high-resolution scanning electron microscope (HRSEM). Optical extinction spectra are recorded using a UV/vis/NIR spectrophotometer (Cary 5000, Agilent). FT-IR spectra are acquired in the reflectance mode (Seagull Variable Angle Reflection Accessory, Harrick) using a Nicolet 8700 FT-IR spectrometer (Thermo Scientific). The spectral response of prepared samples is measured on a FluoroLog-3 fluorescence spectrometer (Jobin-Yvon).

Time-resolved photoluminescence decay curves are also acquired through time-correlated single photon counting methods by using a Fluorolog-3 spectrofluorometer. A 405 nm pulsed diode laser (Picoquant) with a repetition rate of 2.5 MHz is used as the excitation source. The fluorescence signal is obtained through an automated motorized monochromator. Data analyses are performed using a DAS6 software program (Jobin-Yvon). The quality of the fit is assessed by the reduced $\chi 2$ value and visual inspection of the weighted residuals.

Solar Cell Fabrication and Characterization. The counter electrode is prepared by sputtering Au on cleaned FTO glass for 30 s. The photoanode and cathode are assembled in a sandwich type using 25 μm thick thermoplastic sealing film made by Surlyn (Meltonix 1170-25, Solaronix) as a spacer. The electrolyte is prepared by dissolving 0.5 M of Na_2S, 2 M of S, and 0.1 M of NaCl in water and methanol (3:7 vol.).[41]

Electrochemical impedance spectroscopy (EIS) experiments are conducted using a computer-controlled potentiostat (Series G 750, Gamry). EIS is performed in the frequency range between 100 kHz and 100 mHz with an AC voltage amplitude of 10 mV at 0 V vs. V_{OC}. The impedance spectra are interpreted by a nonlinear least-square fitting procedure using commercial software (ZsimpWin). A white light having a light intensity of 30 mW/cm^2 is used as a light source in EIS analyses.

J–*V* characteristics of photovoltaic devices are obtained using a Keithley 2400 source-meter under the illumination of AM 1.5G solar simulated light (1 sun, 100 mW/cm^2, Oriel instruments model 96000, Newport Co.). The light intensity is calibrated with a reference cell and meter (model 91150, Newport Co.).

RESULTS AND DISCUSSION

CdSe QDs are synthesized using a slight modification of a previously reported method.[39] Figure 1a shows TEM images of the CdSe nanocrystals. The size of these highly uniform CdSe QDs is 2.7 ± 0.3 nm in diameter, calculated by statistical analysis of TEM images. Figure 1b shows the absorbance spectrum of the CdSe QDs. The first excitation peak is located at 534 nm, which corresponds to particles with 2.6 nm in diameter.[12] This value is in a good agreement with the diameter of CdSe QDs measured from TEM imaging.

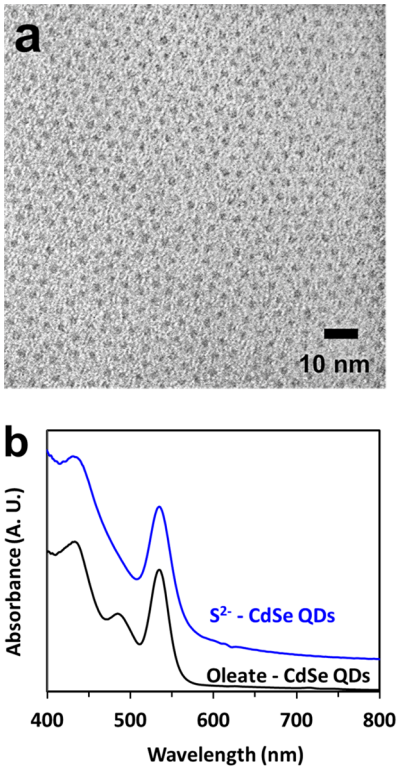

Figure 1. (a) TEM image of the as-synthesized CdSe QDs. Their average diameter is 2.7 ± 0.3 nm. (b) Absorbance spectra of as-synthesized CdSe QDs in toluene and S^{2-}-capped CdSe QDs in formamide.

It is well-known that various nanoparticles having different morphologies can be uniformly deposited by electrophoretic deposition (EPD).[22] Hence, to fabricate a QD-based photoanode, we deposit CdSe QDs on the TiO_2/fluorinated tin oxide (FTO) electrode by EPD.[23] EPD enables CdSe QDs to be deposited into mesoporous TiO_2 with almost continuous coverage over entire electrode.[20−23] Before deposition of CdSe QDs, mesoporous TiO_2 on FTO is fabricated by modifying a published method.[40] The electrophoretic bath is prepared by mixing 40 ml of the oleate capped-CdSe QDs toluene stock solution (10^{-5} M) and 50 ml of acetonitrile. TiO_2/FTO and

FTO electrodes were connected to the positive and negative terminals, respectively, of the power supply. The electrodes are immersed in the prepared QDs solution bath while keeping at a distance of 1 cm apart. 100 V of DC voltage is applied for 10 min to deposit the QDs onto TiO_2, and the electrodes are then rinsed with toluene to remove excess CdSe QDs. We repeat this cycle 6 times. Figure 2a shows the scanning electron

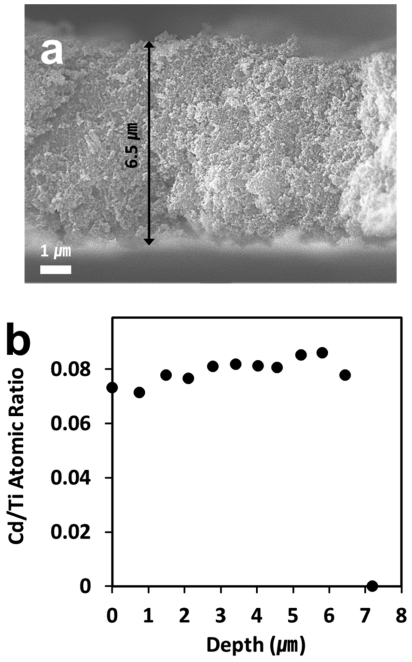

Figure 2. (a) SEM image of a cross section of CdSe/TiO_2/FTO electrode prepared by electrophoretic deposition. (b) EDS depth profile of Cd/Ti ratio in CdSe/TiO_2/FTO electrode.

microscope (SEM) image of a cross-section of the CdSe/TiO_2/FTO electrode. The thickness of the TiO_2 layer on FTO is about 6.5 μm. Energy dispersive X-ray spectroscopy (EDS) shows the Ti/Cd atomic ratio is maintained at about 0.08 throughout the entire TiO_2 cross-section (Figure 2b).

Next, the ligand exchanges of the QDs-deposited photoanode are performed by dipping into the MPA, TGA, and K_2S solutions, typically for an hour. Fourier transform infrared (FT-IR) spectroscopy reveals that oleate-capped CdSe QDs shows sp^3 C−H stretching peaks at 2858 (CH_2-symmetric), 2924 cm^{-1} (CH_3-symmetric), and 2954 cm^{-1} (CH_3-asymmetric) due to the long hydrocarbon bonds in oleate ligands (Figure 3). After ligand exchange with MPA, TGA, and S^{2-}, sp^3 C−H stretching peaks are significantly reduced because of the substitution of short chain ligands on the surfaces. We scraped off the CdSe/TiO_2 from the FTO electrodes for TEM characterization. As shown in Figure S1a in the Supporting Information, CdSe QDs (arrows) are well-deposited on the surface of TiO_2 by EPD. Importantly, their shape and size does not change noticeably after ligand exchange by using S^{2-} (see Figure S1b in the Supporting Information). In addition, we perform the ligand exchange in a solution state in order to further examine the effect of S^{2-}-capping on the size and shape of the CdSe QDs. The native organic ligand of CdSe QDs is exchanged to S^{2-} ions by mixing 1 mL of colloidal CdSe QDs solution and 1 mL of K_2S solution (5 mg/mL) as described in a previous report.[27] Phase transfer of CdSe QDs from toluene to the formamide phase is observed after stirring for 30 min.

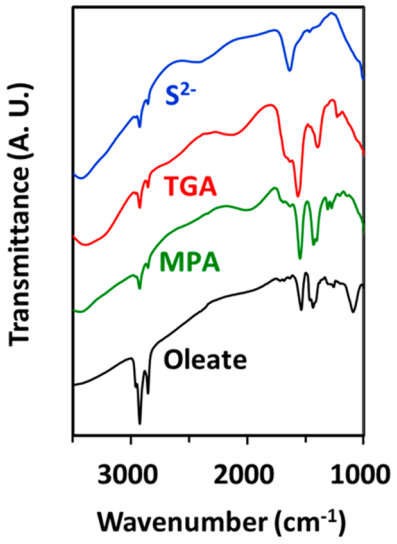

Figure 3. FT-IR spectra of oleate, MPA, TGA, and S^{2-}-capped CdSe QDs on TiO_2.

There was no significant change in the size or shape of the CdSe QDs after ligand exchange as demonstrated by microscopic analysis (see Figure S2 in the Supporting Information). This is further confirmed by the preservation of the original excitonic peak in absorbance spectrum (Figure 1b).

The ligand-dependent electron coupling between CdSe QDs and TiO_2 is investigated by absorbance spectroscopy experiments. Figure 4 shows the absorbance spectra of the oleate,

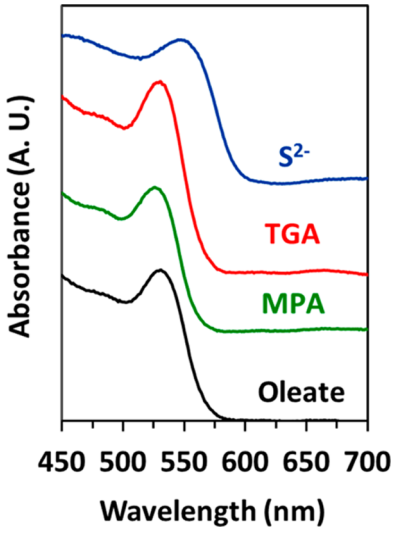

Figure 4. Absorbance spectra of oleate, MPA, TGA, and S^{2-}-capped CdSe QDs on TiO_2.

MPA, TGA, and S^{2-}-capped CdSe/TiO_2 photoanode. The first excitonic peak of oleate-capped CdSe QDs on TiO_2 is located at 534 nm, which is identical to the sample in solution. The position of the first excitonic peak of the QDs does not change after ligand exchange with MPA or TGA. This indicates that the there is no discernible change in size and shape of the CdSe QDs during the ligand exchange. After ligand exchange using the S^{2-} ion, however, the first excitonic peak shifts slightly towards longer wavelengths. As shown in Figure 1b, this red-shift is not observed when oleate ligands on the surface of the

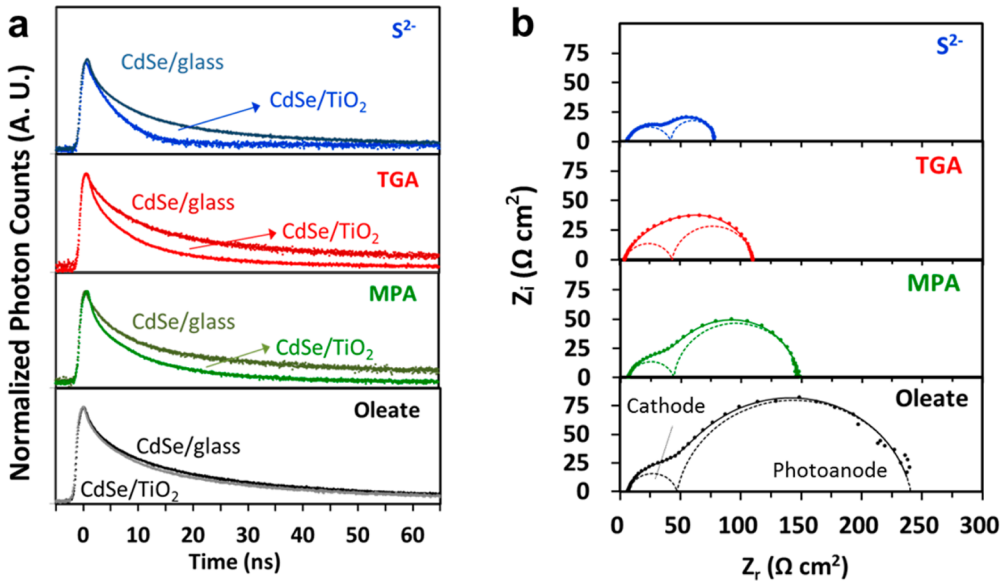

Figure 5. Studies of the charge transfer kinetics at the interfacial region. (a) Decay profile of the photoluminescence from oleate, MPA, TGA, and S^{2-}-capped CdSe QDs on glass and TiO_2. Decays are monitored at the wavelength of the fluorescence peak maximum (oleate, MPA-, and TGA-capped, 554 nm; S^{2-}-capped, 575 nm). (b) Nyquist plots for each QDSSC using oleate, MPA, TGA, and S^{2-}-capped CdSe/TiO_2 as photoanode, respectively, under the illumination of white light (30 mW/cm^2). Symbols and solid lines indicate the experimental data and fitted curves, respectively. Dashed lines are the deconvoluted spectra, which is extracted from simulated results. A gold sputtered FTO glass is used as a counter electrode. The mixed solution of water and methanol (3:7 vol.) of 0.5 M of Na_2S, 2 M of S, and 0.1 M of NaCl served as Red/Ox coupling electrolyte.

CdSe QDs are exchanged with S^{2-} in the solution phase without the TiO_2 substrate. It could be attributed to the enhancement of the electronic coupling between the short S^{2-}-capped CdSe QDs and TiO_2 substrate.[42] The S^{2-} ligand directly contacts the CdSe QDs and TiO_2 without any insulating gap, resulting in enhanced electronic coupling between the QDs and TiO_2. This enhancement can facilitate injection of the photo-generated electron from CdSe QDs to TiO_2.

The enhancement of electronic coupling can be further investigated by time-resolved photoluminescence (TRPL) experiments. The internal charge transfer rate constants (k_{et}) between CdSe QDs and TiO_2 of the oleate, MPA, TGA, and S^{2-}-capped CdSe/TiO_2 photoanode are calculated from the TRPL experiment using a 405 nm monochromatic laser to excite the QDs. The emission decays are monitored at the emission maximum (oleate, MPA-, and TGA-capped, 554 nm; S^{2-}-capped, 575 nm). To study the electron transfer rate, we compare the decay behavior of photo-generated electrons in CdSe QDs deposited on two different substrates, TiO_2, and glass. An electron generated in CdSe QDs is injected into the conduction band of TiO_2 in the photoanode while no electron transfer occurs in the QDs coated on glass. It is assumed that other deactivation processes of photo-excited electrons of as-prepared and ligand-exchanged quantum dots are identical on TiO_2 and glass. This is supported by the fact that the oleate-capped quantum dots deposited on TiO_2 and glass show the similar decay patterns in TRPL experiments. k_{et} can be estimated by comparing the lifetime of electrons generated in CdSe QDs on TiO_2 and glass. Figure 5a displays emission decay profiles of QDs photoanodes treated with different ligands. The fluorescence decay can be fitted to a bi-exponential function using eq 1.[20,43]

$$I(t) = A_1\exp\left(-\frac{t}{\tau_1}\right) + A_2\exp\left(-\frac{t}{\tau_2}\right) \quad (1)$$

This generates two lifetime values, τ_1 and τ_2, with corresponding amplitudes, A_1 and A_2. Then, the intensity-average life time, $\langle\tau\rangle$, is calculated by using the parameters obtained from eq 1, followed by

$$\langle\tau\rangle = \frac{A_1\tau_1^2 + A_2\tau_2^2}{A_1\tau_1 + A_2\tau_2} \quad (2)$$

Finally, k_{et} is estimated from eq 3,

$$k_{et} = \frac{1}{\langle\tau\rangle_{TiO_2}} - \frac{1}{\langle\tau\rangle_{glass}} \quad (3)$$

where $\langle\tau\rangle_{TiO_2}$ and $\langle\tau\rangle_{glass}$ are the intensity-averaged lifetime of the photo-generated electrons in CdSe QDs on TiO_2 and glass, respectively. k_{et} is presented in Table 1 and all fitting results are summarized in Table S1 in the Supporting Information. k_{et} of oleate-capped CdSe/TiO_2 photoanode is 1.03×10^7 s^{-1}. The values of k_{et} remarkably increase after surface modifications

Table 1. Internal Charge Transfer Rate Constants (k_{et}) between CdSe QDs and TiO_2, Charge Transfer Resistance of Photoanode, and Photoelectrochemical Parameters for Each QDSSC Using Oleate, MPA, TGA, and S^{2-}-Capped CdSe/TiO_2 as Photoanode

ligand	k_{et} (s^{-1})	$R_{ct,A}$ (Ω cm^2)	V_{oc} (V)	J_{sc} (mA/cm^2)	FF	η (%)
oleate	1.03×10^7	193.5	0.23	−2.24	0.31	0.16
MPA	2.32×10^7	102.6	0.43	−4.25	0.39	0.72
TGA	5.58×10^7	66.77	0.47	−4.74	0.38	0.85
S^2	1.32×10^8	36.13	0.60	−6.56	0.42	1.65

dx.doi.org/10.1021/am500026a | ACS Appl. Mater. Interfaces 2014, 6, 3721−3728

with shorter chain ligands. Inorganic S^{2-}-capped CdSe QDs shows the most dramatic increase in k_{et}, about 13 times higher (1.32×10^8 s^{-1}) than the value of oleate-capped CdSe/TiO_2 photoanode. In the oleate-capped CdSe/TiO_2, long hydrocarbon chain inhibits transfer of the photo-generated electrons from CdSe QDs to TiO_2, showing the smallest value of k_{et}. The increase in k_{et} in shorter ligands may be due the fact that the barrier to charge transfer resulting from the ligands' long hydrocarbon chains is reduced in the shorter ligand-capped CdSe/TiO_2 (k_{et} of MPA and TGA-capped CdSe/TiO_2 photoanode is 2.32×10^7 and 5.58×10^7, respectively). Specifically the enhancement of electronic coupling in S^{2-}-capped CdSe/TiO_2 photoanode enables photogenerated electrons to be injected faster than the short organic ligand-capped ones.

The overall charge transfer resistance in photoanode devices can be estimated by performing electrochemical impedance spectroscopy (EIS), which is useful in quantifying interfacial electrochemical behaviors of QDSSC,[44,45] DSSC,[46,47] and photoelectrochemical cells.[48] For the EIS measurement, we assemble each photoanode with a Au-sputtered FTO counter electrode using a Surlyn spacer. A polysulfide water/methanol (3:7) solution is used as the Red/Ox coupling electrolyte.[41] In Figure 5b are Nyquist plots for the photovoltaic cell using oleate, MPA, TGA, and S^{2-}-capped CdSe/TiO_2 as the photoanode. Each marker in Figure 5b represents experimental impedance, while the solid lines correspond to theoretical impedance spectra fitted from the electrochemical equivalent circuit shown in Figure S3 in the Supporting Information. The curves of the theoretical simulation are in good agreement with the experimental impedance data, thereby validating the proposed equivalent circuit of this system. The charge transfer resistance of the photoanode ($R_{ct,A}$) and all extracted parameters for each photovoltaic cell are presented in Table 1 and Table S2 in the Supporting Information, respectively. Two semicircles are observed for each Nyquist plot, which are interfacial electrochemical charge transfers on the cathode (at higher frequency) and anode (at lower frequency), respectively.[44,45] Their radius is highly related to the Faradaic Red/Ox charge transfer resistance of each electrode. Any significant change in the radius of the semicircle at higher frequency is not observed within the Nyquist plot for each photovoltaic cell because the Au sputtered counter electrode is used for all experiments, which shows small charge transfer resistance compared to the other interfaces. However, the value of $R_{ct,A}$ decreases remarkably from 193.50 to 36.13 Ω cm^2 with the enhancement of electronic coupling, which indicates the reduction of charge transfer resistance. The advantage of the S^{2-} ligand in internal charge transfer from CdSe QDs to TiO_2 is verified by performing the TRPL experiments. In addition, it is expected that the access of sulfide ion in electrolyte can be improved by employing hydrophilic ligands, MPA, TGA, and S^{2-} ion, compared to ligands with a long hydrocarbon chain, such as oleate-capped CdSe QDs. This leads to the active hole transferring into the electrolyte, by enhancing the oxidation reaction of the sulfide ion in Red/Ox coupling electrolyte to polysulfide ion. In particular, the sulfide ion can be easily oxidized on S^{2-}-capped CdSe QDs due to the smallest charge transfer disturbance, exhibiting the significant decrease in the charge transfer resistance.

To investigate the effect of the charge transfer rate on the photovoltaic performance of QDSSC, the current density-voltage (J–V) characteristics are examined for oleate, MPA, TGA, and S^{2-}-capped photovoltaic cells under the illumination of AM 1.5G solar simulated light (Figure 6a). The short circuit

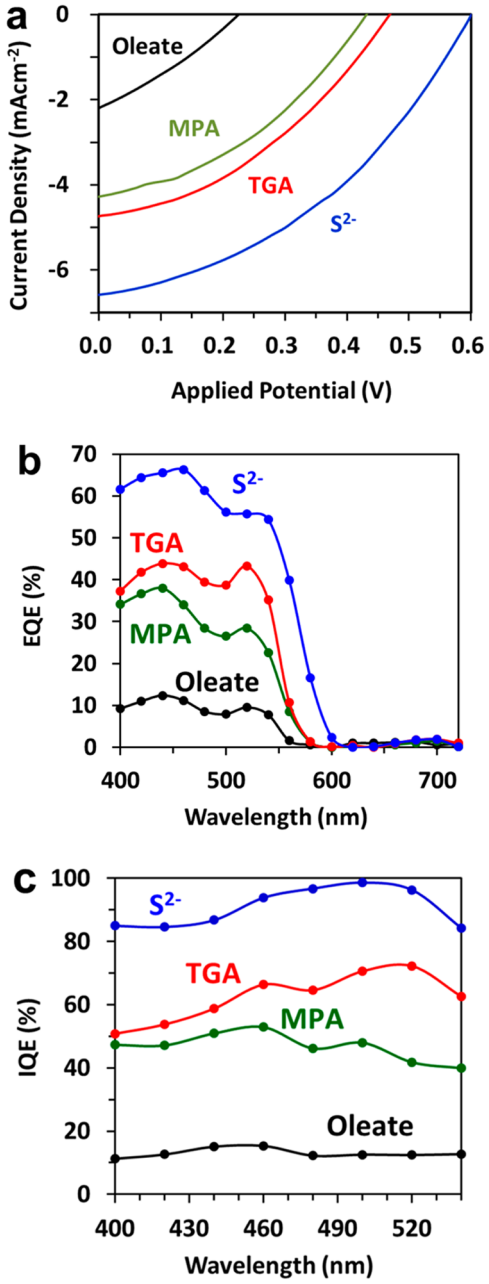

Figure 6. (a) J–V characteristics for each QDSSC under the irradiation of AM 1.5 with an incident power of 100 mW/cm^2. (b) External and (c) internal quantum efficiencies for each QDSSC. A gold sputtered FTO glass is used as a counter electrode. The mixed solution of water and methanol (3:7 vol.) of 0.5 M of Na_2S, 2 M of S, and 0.1 M of NaCl served as Red/Ox coupling electrolyte.

current density (J_{sc}), open circuit voltage (V_{oc}), fill factor (FF), and overall efficiency of power conversion (η) are summarized in Table 1. The QDSSC with oleate-capped CdSe/TiO_2 photoanode shows the lowest solar cell performance because of the long hydrocarbon barrier. J_{sc}, V_{oc}, and η tend to increase with increasing charge transfer kinetics. In particular, S^{2-}-capped CdSe QDs exhibits much higher efficiency (η = 1.65 %) than MPA (η = 0.72 %) or TGA-capped sample (η = 0.85 %), with higher values of J_{sc} (−6.56 mA/cm^2), V_{oc} (0.60 V), and FF

dx.doi.org/10.1021/am500026a | ACS Appl. Mater. Interfaces 2014, 6, 3721−3728

(0.42). This trend is consistent with the results observed in TRPL and EIS measurements, which supports that S^{2-} ligands shorter than MPA and TGA indeed affect the further decrease of the charge transfer barrier resulting in the enhancement of overall solar cell performance.

To further understand the photovoltaic cell performance of QDSSCs, we conducted external and internal quantum efficiency measurement. Figure 6b shows external quantum efficiencies (EQE) of oleate, MPA, TGA, and S^{2-}-capped photovoltaic cells. EQE is calculated by measuring the photocurrent of each cell at different monochromatic excitations. Photocurrent action spectra match well with absorbance spectra of the corresponding photoanode, which are presented in Figure 4. The QDSSC with oleate-capped CdSe/TiO_2 photoanode shows the lowest value of $EQE_{520\ nm}$ (9.5 %). EQE increases significantly with increasing charge transfer kinetics. In particular, S^{2-}-capped CdSe QDs leads to much higher value of $EQE_{520\ nm}$ (55.8 %) than MPA (28.4 %) or TGA-capped sample (43.3 %). In order to examine the ligand-dependence of the electron injection, internal quantum efficiency (IQE) is calculated by dividing the EQE by the absorbance (Figure 6c). IQE also increases significantly with increasing charge transfer kinetics. Interestingly, S^{2-}-capped sample shows a remarkably high value of IQE around 90 % at the range between 400 and 540 nm. This enhancement is caused by high charge transfer rate at the interfacial region, which is verified by TRPL and EIS experiments. The synergic effect of good electronic coupling between CdSe QDs and TiO_2, and the active oxidation reaction of the sulfide ion on the S^{2-}-capped CdSe QDs leads to the remarkable improvement of photovoltaic performance under the irradiation of solar light.

CONCLUSIONS

In summary, we investigated the effect of ligand type on the charge transfer rate and consequently photovoltaic performance in QDSSC by exchanging the native long chain (oleate) ligands of CdSe QD to shorter MPA and TGA and to atomic S^{2-} via solid exchange. TRPL and EIS results show that charge transfer rate at the interfacial region for both CdSe/TiO_2 and the CdSe/polysulfide electrolyte interface increase with enhancing electron coupling. This enhancement of the charge transfer rate leads to effective higher photovoltaic performance of QDSSC. In particular, atomic-sized ligand passivation by using S^{2-} significantly improves solar cell performance because of a faster charge transfer rate. These findings show a new strategy for improving QDSSC performance. This enables the various semiconductor QDs to be more extensively applied to photovoltaic devices by eliminating the barrier of charge transfer because of the long organic chains. Further investigations to improve QDSSC performance and explorations directed toward potential applications are currently in progress.

ASSOCIATED CONTENT

Supporting Information

TEM images of oleate and S^{2-}-capped CdSe/TiO_2, TEM image of S^{2-}-capped CdSe QDs, equivalent electric circuit of the electrochemical system for the quantum dot sensitized solar cell, kinetic analysis of emission decay for each photoanode, and parameters extracted from fitted results of EIS spectra for each QDSSC. This material is available free of charge via the Internet at http://pubs.acs.org.

AUTHOR INFORMATION

Corresponding Author

*E-mail: cbmurray@sas.upenn.edu.

Notes

The authors declare no competing financial interest.

ACKNOWLEDGMENTS

H.J.Y. and C.B.M. acknowledge support from the U.S. Department of Energy Office of Basic Energy Sciences, Division of Materials Science and Engineering (Award DE-SC0002158). This research was also supported by the Basic Science Research Program through the National Research Foundation of Korea (NRF) funded by the Ministry of Education (NRF-2012R1A6A3A03039474). T-J.P. was supported by the Office of Naval Research Multidisciplinary University Research Initiative Award No. ONR-N00014-10-1-0942. C.B.M. is grateful for the support of Richard Perry University Professorship. J.B.B. acknowledges support from an NSF CAREER Award (CBET-0846464). C.B.M. and J.B.B acknowledge support from a collaborative NSF grant (NSF CBET-1335821 for C.B.M. and NSF CBET-1333649 for J.B.B.).

REFERENCES

(1) Kamat, P. V. Quantum Dot Solar Cells. Semiconductor Nanocrystals as Light Harvesters. *J. Phys. Chem. C* **2008**, *112*, 18737−18753.

(2) Kamat, P. V.; Tvrdy, K.; Baker, D. R.; Radich, J. G. Beyond Photovoltaics: Semiconductor Nanoarchitectures for Liquid-Junction Solar Cells. *Chem. Rev.* **2010**, *110*, 6664−6688.

(3) Leschkies, K. S.; Divakar, R.; Basu, J.; Enache-Pommer, E.; Boercker, J. E.; Carter, C. B.; Kortshagen, U. R.; Norris, D. J.; Aydil, E. S. Photosensitization of ZnO Nanowires with CdSe Quantum Dots for Photovoltaic Devices. *Nano Lett.* **2007**, *7*, 1793−1798.

(4) Lee, H.; Wang, M.; Chen, P.; Gamelin, D. R.; Zakeeruddin, S. M.; Graetzel, M.; Nazeeruddin, M. K. Efficient CdSe Quantum Dot-Sensitized Solar Cells Prepared by an Improved Successive Ionic Layer Adsorption and Reaction Process. *Nano Lett.* **2009**, *9*, 4221−4227.

(5) Sun, W. T.; Yu, A.; Pan, H. Y.; Gao, X. F.; Chen, Q.; Peng, L. M. CdS Quantum Dots Sensitized TiO_2 Nanotube-Array Photoelectrodes. *J. Am. Chem. Soc.* **2008**, *130*, 1124−1125.

(6) McDaniel, H.; Fuke, N.; Pietryga, J. M.; Klimov, V. I. Engineered $CuInSe_xS_{2-x}$ Quantum Dots for Sensitized Solar Cells. *J. Phys. Chem. Lett.* **2013**, *4*, 355−361.

(7) Peng, X.; Manna, L.; Yang, W.; Wickham, J.; Scher, E.; Kadavanich, A.; Alivisatos, A. P. Shape Control of CdSe Nanocrystals. *Nature* **2000**, *404*, 59−61.

(8) Alivisatos, A. P. Semiconductor Clusters, Nanocrystals, and Quantum Dots. *Science* **1996**, *271*, 933−937.

(9) Murray, C. B.; Norris, D. J.; Bawendi, M. G. Synthesis and Characterization of Nearly Monodisperse CdE (E = S, Se, Te) Semiconductor Nanocrystallites. *J. Am. Chem. Soc.* **1993**, *115*, 8706−8715.

(10) Robel, I.; Kuno, M.; Kamat, P. V. Size-Dependent Electron Injection from Excited CdSe Quantum Dots into TiO_2 Nanoparticles. *J. Am. Chem. Soc.* **2007**, *129*, 4136−4137.

(11) Rajh, T.; Mićić, O. I.; Nozik, A. J. Synthesis and Characterization of Surface-Modified Colloidal CdTe Quantum Dots. *J. Phys. Chem.* **1993**, *97*, 11999−12003.

(12) Yu, W. W.; Qu, L.; Guo, W.; Peng, X. Experimental Determination of the Extinction Coefficient of CdTe, CdSe, and CdS Nanocrystals. *Chem. Mater.* **2003**, *15*, 2854−2860.

(13) Santra, P. K.; Kamat, P. V. Mn-Doped Quantum Dot Sensitized Solar Cells: A Strategy to Boost Efficiency over 5%. *J. Am. Chem. Soc.* **2012**, *134*, 2508−2511.

(14) Lee, H.; Leventis, H. C.; Moon, S. J.; Chen, P.; Ito, S.; Haque, S. A.; Torres, T.; Nüesch, F.; Geiger, T.; Zakeeruddin, S. M.; Grätzel, M.; Nazeeruddin, M. K. PbS and CdS Quantum Dot-Sensitized Solid-State Solar Cells: "Old Concepts, New Results. *Adv. Funct. Mater.* **2009**, *19*, 2735−2742.
(15) Ardalan, P.; Brennan, T. P.; Lee, H. B. R.; Bakke, J. R.; Ding, I. K.; McGehee, M. D.; Bent, S. F. Effects of Self-Assembled Monolayers on Solid-State CdS Quantum Dot Sensitized Solar Cells. *ACS Nano* **2011**, *5*, 1495−1504.
(16) Zewdu, T.; Clifford, J. N.; Hernández, J. P.; Palomares, E. Photo-Induced Charge Transfer Dynamics in Efficient TiO_2/CdS/CdSe Sensitized Solar Cells. *Energy Environ. Sci.* **2011**, *4*, 4633−4638.
(17) Braga, A.; Giménez, S.; Concina, I.; Vomiero, A.; Mora-Seró, I. Panchromatic Sensitized Solar Cells Based on Metal Sulfide Quantum Dots Grown Directly on Nanostructured TiO_2 Electrodes. *J. Phys. Chem. Lett.* **2011**, *2*, 454−460.
(18) Lee, Y. L.; Lo, Y. S. Highly Efficient Quantum-Dot-Sensitized Solar Cell Based on Co-Sensitization of CdS/CdSe. *Adv. Funct. Mater.* **2009**, *19*, 604−609.
(19) Chang, C. H.; Lee, Y. L. Chemical Bath Deposition of CdS Quantum Dots onto Mesoscopic TiO_2 Films for Application in Quantum-Dot-Sensitized Solar Cells. *Appl. Phys. Lett.* **2007**, *91*.
(20) Santra, P. K.; Kamat, P. V. Tandem-Layered Quantum Dot Solar Cells: Tuning the Photovoltaic Response with Luminescent Ternary Cadmium Chalcogenides. *J. Am. Chem. Soc.* **2013**, *135*, 877−885.
(21) Salant, A.; Shalom, M.; Hod, I.; Faust, A.; Zaban, A.; Banin, U. Quantum Dot Sensitized Solar Cells with Improved Efficiency Prepared Using Electrophoretic Deposition. *ACS Nano* **2010**, *4*, 5962−5968.
(22) Salant, A.; Shalom, M.; Tachan, Z.; Buhbut, S.; Zaban, A.; Banin, U. Quantum Rod-Sensitized Solar Cell: Nanocrystal Shape Effect on the Photovoltaic Properties. *Nano Lett.* **2012**, *12*, 2095−2100.
(23) Chen, J.; Lei, W.; Li, C.; Zhang, Y.; Cui, Y.; Wang, B.; Deng, W. Flexible Quantum Dot Sensitized Solar Cell by Electrophoretic Deposition of CdSe Quantum Dots on ZnO Nanorods. *Phys. Chem. Chem. Phys.* **2011**, *13*, 13182−13184.
(24) Watson, D. F. Linker-Assisted Assembly and Interfacial Electron-Transfer Reactivity of Quantum Dot-Substrate Architectures. *J. Phys. Chem. Lett.* **2010**, *1*, 2299−2309.
(25) Pernik, D. R.; Tvrdy, K.; Radich, J. G.; Kamat, P. V. Tracking the Adsorption and Electron Injection Rates of CdSe Quantum Dots on TiO_2: Linked Versus Direct Attachment. *J. Phys. Chem. C* **2011**, *115*, 13511−13519.
(26) Majidi, H.; Winkler, C. R.; Taheri, M. L.; Baxter, J. B. Microstructural Changes in CdSe-Coated ZnO Nanowires Evaluated by in Situ Annealing in Transmission Electron Microscopy and X-Ray Diffraction. *Nanotechnology* **2012**, *23*.
(27) Nag, A.; Kovalenko, M. V.; Lee, J. S.; Liu, W.; Spokoyny, B.; Talapin, D. V. Metal-Free Inorganic Ligands for Colloidal Nanocrystals: S^{2-}, HS^-, Se^{2-}, HSe^-, Te^{2-}, HTe^-, TeS_3^{2-}, OH^-, and NH^{2-} as Surface Ligands. *J. Am. Chem. Soc.* **2011**, *133*, 10612−10620.
(28) Chung, D. S.; Lee, J. S.; Huang, J.; Nag, A.; Ithurria, S.; Talapin, D. V. Low Voltage, Hysteresis Free, and High Mobility Transistors from All-Inorganic Colloidal Nanocrystals. *Nano Lett.* **2012**, *12*, 1813−1820.
(29) Nag, A.; Chung, D. S.; Dolzhnikov, D. S.; Dimitrijevic, N. M.; Chattopadhyay, S.; Shibata, T.; Talapin, D. V. Effect of Metal Ions on Photoluminescence, Charge Transport, Magnetic and Catalytic Properties of All-Inorganic Colloidal Nanocrystals and Nanocrystal Solids. *J. Am. Chem. Soc.* **2012**, *134*, 13604−13615.
(30) Tang, J.; Kemp, K. W.; Hoogland, S.; Jeong, K. S.; Liu, H.; Levina, L.; Furukawa, M.; Wang, X.; Debnath, R.; Cha, D.; Chou, K. W.; Fischer, A.; Amassian, A.; Asbury, J. B.; Sargent, E. H. Colloidal-Quantum-Dot Photovoltaics Using Atomic-Ligand Passivation. *Nat. Mater.* **2011**, *10*, 765−771.
(31) Fafarman, A. T.; Koh, W. K.; Diroll, B. T.; Kim, D. K.; Ko, D. K.; Oh, S. J.; Ye, X.; Doan-Nguyen, V.; Crump, M. R.; Reifsnyder, D. C.; Murray, C. B.; Kagan, C. R. Thiocyanate-Capped Nanocrystal Colloids: Vibrational Reporter of Surface Chemistry and Solution-Based Route to Enhanced Coupling in Nanocrystal Solids. *J. Am. Chem. Soc.* **2011**, *133*, 15753−15761.
(32) Stolle Jackson, C.; Panthani, M. G.; Harvey, T. B.; Akhavan, V. A.; Korgel, B. A. Comparison of the Photovoltaic Response of Oleylamine and Inorganic Ligand-Capped $CuInSe_2$ Nanocrystals. *ACS Appl. Mater. Interfaces* **2012**, *4*, 2757−2761.
(33) Li, L.; Yang, X.; Gao, J.; Tian, H.; Zhao, J.; Hagfeldt, A.; Sun, L. Highly Efficient CdS Quantum Dot-Sensitized Solar Cells Based on a Modified Polysulfide Electrolyte. *J. Am. Chem. Soc.* **2011**, *133*, 8458−8460.
(34) Pan, Z.; Zhang, H.; Cheng, K.; Hou, Y.; Hua, J.; Zhong, X. Highly Efficient Inverted Type-I CdS/CdSe Core/Shell Structure QD-Sensitized Solar Cells. *ACS Nano* **2012**, *6*, 3982−3991.
(35) Zhang, H.; Cheng, K.; Hou, Y. M.; Fang, Z.; Pan, Z. X.; Wu, W. J.; Hua, J. L.; Zhong, X. H. Efficient CdSe Quantum Dot-Sensitized Solar Cells Prepared by a Postsynthesis Assembly Approach. *Chem. Commun.* **2012**, *48*, 11235−11237.
(36) Kuo, C. Y.; Su, M. S.; Ku, C. S.; Wang, S. M.; Lee, H. Y.; Wei, K. H. Ligands Affect the Crystal Structure and Photovoltaic Performance of Thin Films of PbSe Quantum Dots. *J. Mater. Chem.* **2011**, *21*, 11605−11612.
(37) De La Fuente, M. S.; Sánchez, R. S.; González-Pedro, V.; Boix, P. P.; Mhaisalkar, S. G.; Rincón, M. E.; Bisquert, J.; Mora-Seró, I. Effect of Organic and Inorganic Passivation in Quantum-Dot-Sensitized Solar Cells. *J. Phys. Chem. Lett.* **2013**, *4*, 1519−1525.
(38) Wang, H.; Luan, C.; Xu, X.; Kershaw, S. V.; Rogach, A. L. In Situ versus Ex Situ Assembly of Aqueous-Based Thioacid Capped CdSe Nanocrystals within Mesoporous TiO_2 Films for Quantum Dot Sensitized Solar Cells. *J. Phys. Chem. C* **2012**, *116*, 484−489.
(39) Jasieniak, J.; Bullen, C.; Van Embden, J.; Mulvaney, P. Phosphine-Free Synthesis of CdSe Nanocrystals. *J. Phys. Chem. B* **2005**, *109*, 20665−20668.
(40) Ito, S.; Chen, P.; Comte, P.; Nazeeruddin, M. K.; Liska, P.; Péchy, P.; Graetzel, M. Fabrication of Screen-Printing Pastes from TiO_2 Powders for Dye-Sensitised Solar Cells. *Prog. Photovoltaics* **2007**, *15*, 603−612.
(41) Lee, Y. L.; Chang, C. H. Efficient Polysulfide Electrolyte for CdS Quantum Dot-Sensitized Solar Cells. *J. Power Sources* **2008**, *185*, 584−588.
(42) Tisdale, W. A.; Williams, K. J.; Timp, B. A.; Norris, D. J.; Aydil, E. S.; Zhu, X. Y. Hot-Electron Transfer from Semiconductor Nanocrystals. *Science* **2010**, *328*, 1543−1547.
(43) Chen, Y. C.; Pu, Y. C.; Hsu, Y. J. Interfacial Charge Carrier Dynamics of the Three-Component In_2O_3-TiO_2-Pt Heterojunction System. *J. Phys. Chem. C* **2012**, *116*, 2967−2975.
(44) González-Pedro, V.; Xu, X.; Mora-Seró, I.; Bisquert, J. Modeling High-Efficiency Quantum Dot Sensitized Solar Cells. *ACS Nano* **2010**, *4*, 5783−5790.
(45) Jung, M. H.; Kang, M. G. Enhanced Photo-Conversion Efficiency of CdSe-ZnS Core-Shell Quantum Dots with Au Nanoparticles on TiO_2 Electrodes. *J. Mater. Chem.* **2011**, *21*, 2694−2700.
(46) Halme, J.; Vahermaa, P.; Miettunen, K.; Lund, P. Device Physics of Dye Solar Cells. *Adv. Mater.* **2010**, *22*, E210−E234.
(47) Fabregat-Santiago, F.; Bisquert, J.; Palomares, E.; Otero, L.; Kuang, D.; Zakeeruddin, S. M.; Grätzel, M. Correlation between Photovoltaic Performance and Impedance Spectroscopy of Dye-Sensitized Solar Cells Based on Ionic Liquids. *J. Phys. Chem. C* **2007**, *111*, 6550−6560.
(48) Yun, H. J.; Lee, H.; Joo, J. B.; Kim, W.; Yi, J. Influence of Aspect Ratio of TiO_2 Nanorods on the Photocatalytic Decomposition of Formic Acid. *J. Phys. Chem. C* **2009**, *113*, 3050−3055.